Astronomy & Astrophysics

LETTER TO THE EDITOR

First spectrally-resolved H₂ observations towards HH 54*

Low H₂O abundance in shocks

G. Santangelo[1,2], S. Antoniucci[2], B. Nisini[2], C. Codella[1], P. Bjerkeli[3,4,5], T. Giannini[2], A. Lorenzani[1], L. K. Lundin[6], S. Cabrit[7], L. Calzoletti[8], R. Liseau[5], D. Neufeld[9], M. Tafalla[10], and E. F. van Dishoeck[11,12]

[1] Osservatorio Astrofisico di Arcetri, Largo Enrico Fermi 5, 50125 Florence, Italy
  e-mail: gina@arcetri.astro.it
[2] Osservatorio Astronomico di Roma, via di Frascati 33, 00040 Monteporzio Catone, Italy
[3] Niels Bohr Institute, University of Copenhagen, Juliane Maries Vej 30, 2100 Copenhagen Ø., Denmark
[4] Centre for Star and Planet Formation and Natural History Museum of Denmark, University of Copenhagen, Øster Voldgade 5–7, 1350 Copenhagen K., Denmark
[5] Department of Earth and Space Sciences, Chalmers University of Technology, Onsala Space Observatory, 439 92 Onsala, Sweden
[6] European Southern Observatory, Karl Schwarzschild str.2, 85748 Garching bei Muenchen, Germany
[7] LERMA, Observatoire de Paris, UMR 8112 of the CNRS, 61 Av. de l'Observatoire, 75014 Paris, France
[8] ASDC, 00044 Frascati, Roma, Italy
[9] The Johns Hopkins University, Baltimore, MD 21218, USA
[10] Observatorio Astronómico Nacional (IGN), Alfonso XII 3, 28014 Madrid, Spain
[11] Leiden Observatory, Leiden University, PO Box 9513, 2300 RA Leiden, The Netherlands
[12] Max Planck Institut für Extraterrestrische Physik (MPE), Giessenbachstr.1, 85748 Garching, Germany

ABSTRACT

Context. *Herschel* observations suggest that the H₂O distribution in outflows from low-mass stars resembles the H₂ emission. It is still unclear which of the different excitation components that characterise the mid- and near-IR H₂ distribution is associated with H₂O.
Aims. The aim is to spectrally resolve the different excitation components observed in the H₂ emission. This will allow us to identify the H₂ counterpart associated with H₂O and finally derive directly an H₂O abundance estimate with respect to H₂.
Methods. We present new high spectral resolution observations of H₂ $0-0$ S(4), $0-0$ S(9), and $1-0$ S(1) towards HH 54, a bright nearby shock region in the southern sky. In addition, new *Herschel*/HIFI H₂O ($2_{12}-1_{01}$) observations at 1670 GHz are presented.
Results. Our observations show for the first time a clear separation in velocity of the different H₂ lines: the $0-0$ S(4) line at the lowest excitation peaks at -7 km s^{-1}, while the more excited $0-0$ S(9) and $1-0$ S(1) lines peak at -15 km s^{-1}. H₂O and high-J CO appear to be associated with the H₂ $0-0$ S(4) emission, which traces a gas component with a temperature of $700-1000$ K. The H₂O abundance with respect to H₂ $0-0$ S(4) is estimated to be X(H₂O) $< 1.4 \times 10^{-5}$ in the shocked gas over an area of 13″.
Conclusions. We resolve two distinct gas components associated with the HH 54 shock region at different velocities and excitations. This allows us to constrain the temperature of the H₂O emitting gas ($\leq$1000 K) and to derive correct estimates of H₂O abundance in the shocked gas, which is lower than what is expected from shock model predictions.

Key words. stars: formation – infrared: ISM – ISM: jets and outflows – Herbig-Haro objects – ISM: individual objects: HH 54

1. Introduction

Protostellar jets and outflows are a direct consequence of the accretion mechanism in young stellar objects during their earliest phase (e.g. Ray et al. 2007). The interaction between the ejecta and the circumstellar medium occurs via radiative shocks (e.g. Kaufman & Neufeld 1996; Flower & Pineau des Forêts 2010), whose energy is radiated away through emission lines of atomic, ionic, and molecular species. Hot gas at temperatures above 2000 K cools principally through H₂ ro-vibrational lines in the near-IR and abundant atomic and ionic species (e.g. Eislöffel et al. 2000; Giannini et al. 2004). Warm gas components at hundreds of Kelvin cool via mid- and far-IR molecular lines, particularly rotational transitions of H₂ (at $\lambda \leq 28$ μm) and lines of other molecular species, such as CO and H₂O.

Water has a key role in protostellar environments (van Dishoeck et al. 2011). Its abundance with respect to H₂ is expected to increase from $<10^{-7}$ in cold regions up to 3×10^{-4} in warm gas due to the combined effects of sputtering of grain mantles and high-temperature reactions (Hollenbach & McKee 1989; Kaufman & Neufeld 1996; Flower & Pineau des Forêts 2010; Suutarinen et al. 2014). The *Herschel* Space Observatory revealed the complexity of H₂O line profiles (e.g. Codella et al. 2010; Kristensen et al. 2012; Santangelo et al. 2012; Vasta et al. 2012) and showed that H₂O emission probes warm ($\gtrsim$300 K) and dense ($n_{\rm H_2} > 10^5$ cm^{-3}) gas with spatial distribution that resembles the H₂ emission (e.g. Nisini et al. 2010; Tafalla et al. 2013; Santangelo et al. 2013). Low H₂O abundances are derived in outflows for warm shocked gas, ranging from a few $\times10^{-6}$ to a few $\times10^{-5}$ (e.g. Bjerkeli et al. 2012; Santangelo et al. 2013; Tafalla et al. 2013; Busquet et al. 2014). These abundance values are at least an order of magnitude lower than what is expected in warm shocked gas from shock model predictions (e.g. Kaufman & Neufeld 1996; Flower & Pineau des Forêts 2010). Their determinations rely on the assumption that H₂O traces the same gas as the spectrally unresolved low-J H₂ $0-0$ lines. Spectrally

---

* Based on observations made with ESO telescopes at the La Silla Paranal Observatory under programme IDs: 089.C-0772, 292.C-5025.

Table 1. H_2 transitions observed.

Transition	Wavelength (μm)	$E_{\rm up}$ (K)	Telescope/Instrument	Slit ('')	PA (°)	$R = \lambda/\Delta\lambda$	Δv (km s^{-1})	Date (m, y)	Exposure time (min)
H_2 0−0 S(4)	8.0251	3474	VLT/VISIR	0.4 × 32	−26	32 000	10	Apr. 2012	45
H_2 0−0 S(9)	4.6947	10263	VLT/CRIRES	0.4 × 40	113	50 000	6	Jan./Feb. 2014	102
H_2 1−0 S(1)	2.1218	6956	VLT/CRIRES	0.4 × 40	113	50 000	6	Jan./Feb. 2014	10

resolved observations of H_2 are thus needed to directly compare the line profiles and finally test this hypothesis.

The Herbig-Haro object HH 54 is located in the nearby star-forming region Chamaeleon II (D = 180 pc, Whittet et al. 1997). The object shows a clumpy appearance, consisting of several arcsecond-scale bright knots. Knee (1992) associates HH 54 with a monopolar blue-shifted CO outflow, whose driving source remains unclear (e.g. Caratti o Garatti et al. 2006; Ybarra & Lada 2009; Bjerkeli et al. 2011). Mid-IR cooling is dominated by pure rotational H_2 lines (Cabrit et al. 1999; Giannini et al. 2006; Neufeld et al. 1998, 2006) probing warm gas with a mixture of temperatures in the range 400−1200 K. HH 54 was also observed in several lines of CO and H_2O from space and the ground (Liseau et al. 1996; Nisini et al. 1996; Bjerkeli et al. 2009, 2011).

In this letter we present new ESO VLT high-resolution spectroscopic observations of H_2 towards HH 54. The observations are complemented with *Herschel*/HIFI observations of H_2O ($2_{12}-1_{01}$). This unique dataset is used to spectrally resolve the different excitation components observed in H_2. We are finally able to identify the H_2 counterpart associated with H_2O and derive the H_2O abundance in the shocked gas directly.
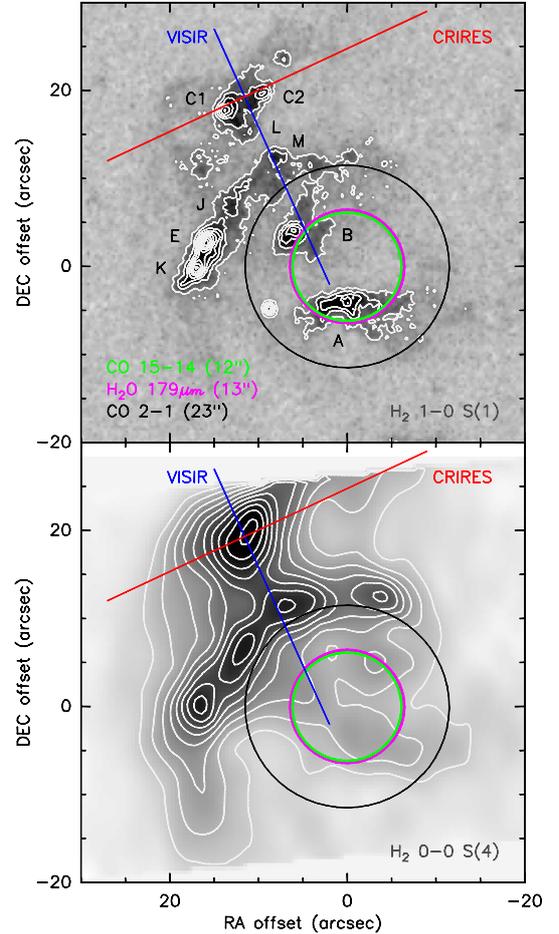
2. Observations

Our dataset consists of data collected towards HH 54 with ESO facilities (Table 1) and with *Herschel*. Figure 1 shows the VLT slit positions and *Herschel* and SEST beam sizes for the observations presented in this paper in comparison with the H_2 1−0 S(1) and 0−0 S(4) maps of the region (Giannini et al. 2006; Neufeld et al. 2006).

2.1. VISIR high-resolution mid-IR spectroscopy

On April 2012 we performed spectrally-resolved observations of H_2 0−0 S(4) (see Table 1) with VLT/VISIR (Lagage et al. 2004). The $0\farcs4 \times 32''$ slit was positioned on the basis of the *Spitzer* image (see Fig. 1); it was oriented in a way to encompass knot B, which was covered by the *Herschel* single-pointing observations of H_2O (see Sect. 2.3), and the C1/C2 knots, which correspond to the brightest knot in the *Spitzer* H_2 emission. We conducted our observations by chopping and nodding the telescope off-source, with equal time on both positions. Data reduction and calibration were performed by using the VISIR pipeline recipes (version 3.5.1)[1], which provide standard procedures for flat-fielding and background subtraction. A model for the sky emission lines is used by the pipeline for the wavelength calibration. To fit the dispersion relation we employed a second degree polynomial, which provides higher correlation coefficient with respect to the default pipeline linear solution. The uncertainty on the peak velocity is about 3 km s^{-1}, comparable with the spectral pixel. The IRAF package was used for spectra extraction. Only

---

[1] https://www.eso.org/sci/software/pipelines/visir/visir-pipe-recipes.html

Fig. 1. *Upper*: H_2 1−0 S(1) image of HH 54 from NTT/SofI observations (Giannini et al. 2006). The positioning of the slits adopted for VLT/VISIR and CRIRES observations is shown in blue and red. The beam sizes of *Herschel* H_2O ($2_{12}-1_{01}$) (magenta circle), CO (15−14) (green, Bjerkeli et al. 2014), and SEST CO (2−1) (black, Bjerkeli et al. 2009, 2011) are displayed. Offsets are relative to: $\alpha_{J2000} = 12^{\rm h}55^{\rm m}50\fs3$, $\delta_{J2000} = -76°56'23''$ (Bjerkeli et al. 2011). *Lower*: *Spitzer*/IRS H_2 0−0 S(4) image of HH 54 (Neufeld et al. 2006). Symbols are the same as in the upper panel.

C1/C2 knots are clearly detected with VISIR; knot M is only tentatively detected in the spectral image, whereas knot B is not detected.

2.2. CRIRES high-resolution near-IR spectroscopy

We carried out high-dispersion spectroscopic observations of the H_2 0−0 S(9) and H_2 1−0 S(1) transitions (Table 1) towards HH 54 with VLT/CRIRES (Kaeufl et al. 2004). Observations were performed between January and February 2014 during director discretionary time. Since only the bright C1/C2 knots were detected by VISIR, the CRIRES $0\farcs4 \times 40''$ slit was oriented

in order to cover them (Fig. 1). Chopping and nodding were performed along the slit to minimise the integration time. Data reduction and wavelength calibration were performed with the CRIRES pipeline recipes (version 2.3.1). The wavelength calibration, based on the comparison with a sky emission model, was satisfactory (high correlation coefficient) for the 0−0 S(9). OH emission lines were used to refine the wavelength scale for the 1−0 S(1). The uncertainty associated with peak velocities is ~2.5 km s^{-1}. The IRAF package was used for spectra extraction.

2.3. Herschel/HIFI observations

Single-pointing observations of H_2O $(2_{12}-1_{01})$ at 1669.9 GHz were performed with the Heterodyne Instrument for the Far Infrared (HIFI, de Graauw et al. 2010) on board *Herschel* towards HH 54B (see Fig. 1). The reference coordinates are α_{J2000} = 12^{h}55^{m}50$.\!^s$3, δ_{J2000} = −76°56′23″. The observations were carried out in September 2012[2]. The diffraction-limited beam size is ~13″. The data were processed with the ESA-supported package HIPE version 12.0 for calibration. The HebCorrection and fitHifiFringe tasks within HIPE were successfully used to remove the electronic standing waves in Band 6, which affected the line. Further data reduction and analysis were performed using the GILDAS[3] software. The antenna temperature scale, T_A^*, was converted into the main-beam temperature scale, T_{mb}, using main-beam efficiency factor of 0.71 (Roelfsema et al. 2012). The flux calibration uncertainty is around 10%, based on cross-calibration with *Herschel*/PACS (Bjerkeli et al. 2011). At the velocity resolution of 1 km s^{-1}, the rms noise is 80 mK (T_{mb} scale).

3. Two velocity components in H_2 observations

Velocity centroids of the CRIRES spectra at C1 and C2 knots are consistent within one spectral pixel (<3 km s^{-1}). The two spectra have thus been averaged to compare with VISIR H_2 0−0 S(4) extracted at knot C1/C2. The comparison is presented in the upper panel of Fig. 2. A peak velocity of −7 km s^{-1} is associated with the 0−0 S(4) line, whereas the higher excitation 1−0 S(1) and 0−0 S(9) lines peak at the higher blue-shifted velocity of −15 km s^{-1}. Our spectrally-resolved H_2 observations clearly show for the first time that mid-IR and near-IR H_2 lines are well separated in velocity, thus representing two distinct velocity components. This suggests that two separate shock components with different excitation conditions are associated with gas peaking at different velocities.

The comparison between H_2 0−0 S(4) at HH 54C1/C2 and H_2O $(2_{12}-1_{01})$, CO (15−14) (Bjerkeli et al. 2014), and CO (2−1) (Bjerkeli et al. 2009, 2011) observations at HH 54B is presented in the lower panel of Fig. 2. The low-J CO lines, in particular CO (2−1), present a two-components profile: a triangular-shaped low-velocity (LV CO, hereafter) component, which peaks at the systemic velocity of the cloud (+2.4 km s^{-1}); and an additional superposed "bump-like" component (Bjerkeli et al. 2011) centred at the blue-shifted velocity of −7 km s^{-1}. This latter feature seems to dominate the emission of the high-J CO (15−14). The similarity between CO (15−14) and H_2O line profiles, taken with similar beam sizes (12″ and 13″), suggests that the bump feature is associated with the H_2O emitting gas and has higher excitation with respect to the LV gas.
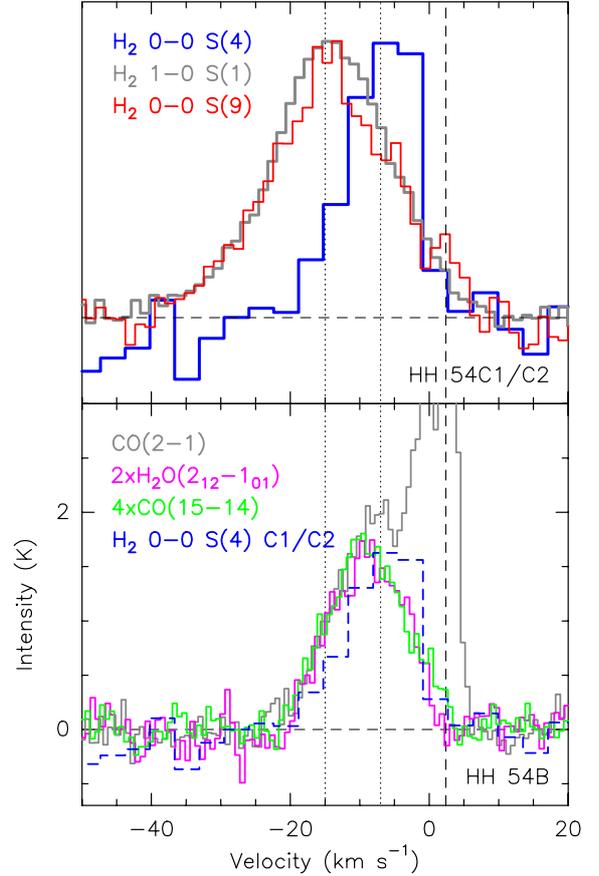
Fig. 2. *Upper*: H_2 0−0 S(4) towards HH 54C1/C2 is compared with 1−0 S(1) and 0−0 S(9). Spectra are normalized to their peak values. The vertical dashed line marks the systemic velocity (v_{LSR} = +2.4 km s^{-1}, Bjerkeli et al. 2011). The two vertical dotted lines indicate the velocity of: the 0−0 S(4) peak at −7 km s^{-1}; and the 1−0 S(1) and 0−0 S(9) peaks at −15 km s^{-1}. *Lower*: H_2O $(2_{12}-1_{01})$, CO (15−14), and CO (2−1) towards HH 54B are compared with H_2 0−0 S(4) at HH 54C1/C2. H_2O, CO, and H_2 are normalized to the peak of the bump feature in CO (2−1).

Although the H_2 0−0 S(4) spectrum is taken at the C1/C2 knot, the comparison with H_2O and high-J CO observed at knot B shows that the three lines trace emission in the same velocity range. Moreover, taking the different spectral resolutions and the uncertainty on the H_2 peak velocity determination into account (see Sect. 2.1), the H_2 0−0 S(4) line profile well resembles the H_2O and high-J CO line profiles (Fig. 2 bottom). HIFI maps of CO (10−9) and lower-J CO lines by Bjerkeli et al. (2011) show that, although the relative intensity of the LV and bump components changes within the HH 54 region, their peak velocities remain constant within 2 km s^{-1} among the different knots. We thus also assume that the peak velocity of the H_2O emission, which appears to be associated with the high-J CO emission at knot B, does not change within the region and in particular along the VISIR slit. In this case, the H_2 0−0 S(4) emission would be associated with the same gas as traced by H_2O and high-J CO.

In conclusion, our observations detect for the first time the presence of a stratification in velocity in the H_2 gas from low- to high-excitation emission lines. The H_2 0−0 S(4) component appears to be associated with H_2O and high-J CO, as expected from the comparison between the spatial distributions (e.g. Nisini et al. 2010; Tafalla et al. 2013; Santangelo et al. 2013). We note that in the low-J CO an additional gas

---

[2] The data are part of the OT2 program "Herschel observations of the shocked gas in HH 54" (observation ID: 1342251604).
[3] http://www.iram.fr/IRAMFR/GILDAS/

component around the systemic velocity is detected. This gas component is not observed in the high-J CO lines and in the H_2 lines, since higher temperatures are needed to excite them. On the other hand, the higher velocity component associated with H_2 1−0 S(1) and 0−0 S(9) is not detected in the CO emission, even in the higher-J lines, since it is associated with a gas at even higher temperatures ($T \gtrsim 2000$ K).

4. H₂O abundance estimate

Our new observations allow us to spectrally identify the 0−0 S(4) line as the H_2 counterpart associated with H_2O, with the assumption that the H_2 and H_2O profiles do not change between the C and B knots. This can be used to accurately constrain the temperature of the gas from the H_2 emission and derive correct H_2O abundances with respect to H_2. Neufeld et al. (2006) mapped H_2 S(0)−S(7) pure rotational lines towards HH 54 with *Spitzer*/IRS. Their H_2 rotational diagram, constructed over a 15″ region encompassing HH 54B, indicates the presence of warm gas with temperatures in the range 400−1200 K. According to these authors, a temperature range of 700−1000 K is associated with the 0−0 S(4) emission, which corresponds $N(H_2) = 6.6 \times 10^{19}$ and 2.1×10^{19} cm^{-2} over 13″ for 700 and 1000 K, respectively.

We assumed for the H_2O emission the same temperature range as derived from the H_2 0−0 S(4) line and a gas density $n(H_2) \gtrsim 10^5$ cm^{-3} (e.g. Tafalla et al. 2013; Santangelo et al. 2013; Busquet et al. 2014). We used the RADEX molecular LVG radiative transfer code (van der Tak et al. 2007) to model the observed H_2O ($2_{12}-1_{01}$) emission. A typical line width of 10 km s^{-1} was adopted from a Gaussian fitting to the spectrum (see Fig. 2). The lower limit on the H_2 density corresponds to an upper limit on the derived column density. In particular, we obtain $N(H_2O) < 3 \times 10^{14}$ cm^{-2} over a 13″ area. The comparison with the H_2 column density obtained from the 0−0 S(4) for the same temperature range gives an H_2O abundance $X(H_2O) < 1.4 \times 10^{-5}$. A lower H_2 density of 2×10^4 cm^{-3} (Bjerkeli et al. 2011, 2014) would increase the H_2O abundance by a factor of 2. The upper level energy of H_2O ($2_{12}-1_{01}$), which is about 114 K, is much smaller than that of the H_2 S(4) line (Table 1). Therefore, we cannot exclude that H_2O emission is associated with a colder gas component that is not probed by our H_2 observations. However, a temperature lower than the assumed 700−1000 K would indicate an even lower H_2O abundance, thus strengthening our result. The derived upper limit on the H_2O abundance is in agreement with the abundance value of 10^{-5} derived by Liseau et al. (1996) and Bjerkeli et al. (2011) from ISO and *Herschel* observations of transitions at similar wavelengths as well as with the upper limit of $<1.6 \times 10^{-4}$ obtained by Neufeld et al. (2006) based on non-detections of shorter wavelength transitions covered by *Spitzer*. Our H_2O abundance estimate in HH 54 confirms the values recently found by *Herschel* in outflows from Class 0 sources (e.g. Bjerkeli et al. 2012; Santangelo et al. 2013; Tafalla et al. 2013; Busquet et al. 2014), which are based on the assumption that H_2O traces the same gas as traced by the low-J H_2 emission.

An estimate of the H_2O abundance at the C knot can also be derived using the PACS map of H_2O ($2_{12}-1_{01}$) by Bjerkeli et al. (2011). The H_2O flux density at knot C is a factor of 2 lower than at the position of the HIFI H_2O observations, which yields $N(H_2O) < 10^{14}$ cm^{-2}. The H_2 column density obtained from the 0−0 S(4) at knot C is in the range $N(H_2) = 5 \times 10^{19}$−$1.6 \times 10^{20}$ cm^{-2} for 1000 and 700 K, respectively. The

comparison between H_2O and H_2 indicates an H_2O abundance $X(H_2O) < 2 \times 10^{-6}$, which is even more strict than that derived at knot B. This indicates a variation of H_2O abundance within the HH 54 region, with a decrease towards the peak of the H_2 S(4) emission. This may explain the different emission peaks of the H_2O distribution observed by PACS (Bjerkeli et al. 2011) and the H_2 S(4) emission.

5. Conclusions

We present new spectrally-resolved observations towards HH 54 of H_2 0−0 S(4), 0−0 S(9), and 1−0 S(1). These are complemented by new *Herschel*/HIFI H_2O ($2_{12}-1_{01}$) observations. Our data show for the first time the separation in velocity between the gas component traced by the low-excitation H_2 0−0 S(4) line and that associated with the H_2 lines at higher excitation. The observed H_2 stratification in velocity suggests that our observations resolve two distinct gas components associated with the HH 54 shock region at different velocity and excitation. We spectrally identify the H_2 0−0 S(4) line as the H_2 counterpart of H_2O emission. This allows us to constrain the temperature of the H_2O emitting gas (≤ 1000 K). H_2O abundance is estimated to be lower than what is expected from shock model predictions by at least one order of magnitude. High spectral resolution observations of different targets are needed to confirm this result.

References

Bjerkeli, P., Liseau, R., Olberg, M., et al. 2009, A&A, 507, 1455
Bjerkeli, P., Liseau, R., Nisini, B., et al. 2011, A&A, 533, A80
Bjerkeli, P., Liseau, R., Larsson, B., et al. 2012, A&A, 546, A29
Bjerkeli, P., Liseau, R., Brinch, C., et al. 2014, A&A, in press,
    DOI: 10.1051/0004-6361/201424789
Busquet, G., Lefloch, B., Benedettini, M., et al. 2014, A&A, 561, A120
Cabrit, S., Bontemps, S., et al. 1999, The Universe as Seen by ISO, 427, 449
Caratti o Garatti, A., Giannini, T., Nisini, B., et al. 2006, A&A, 449, 1077
Codella, C., Lefloch, B., Ceccarelli, C., et al. 2010, A&A, 518, L112
de Graauw, T., Helmich, F. P., Phillips, T. G., et al. 2010, A&A, 518, L6
Eislöffel, J., Smith, M. D., & Davis, C. J. 2000, A&A, 359, 1147
Flower, D. R., & Pineau des Forêts, G. 2010, MNRAS, 406, 1745
Giannini, T., McCoey, C., Caratti o Garatti, A., et al. 2004, A&A, 419, 999
Giannini, T., McCoey, C., Nisini, B., et al. 2006, A&A, 459, 821
Hollenbach, D., & McKee, C. F. 1989, ApJ, 342, 306
Kaeufl, H.-U., Ballester, P., Biereichel, P., et al. 2004, Proc. SPIE, 5492, 1218
Kaufman, M. J., & Neufeld, D. A. 1996, ApJ, 456, 611
Knee, L. B. G. 1992, A&A, 259, 283
Kristensen, L. E., van Dishoeck, E. F., Bergin, E. A., et al. 2012, A&A, 542, A8
Lagage, P. O., Pel, J. W., Authier, M., et al. 2004, The Messenger, 117, 12
Liseau, R., Ceccarelli, C., Larsson, B., et al. 1996, A&A, 315, L181
Neufeld, D. A., Melnick, G. J., & Harwit, M. 1998, ApJ, 506, L75
Neufeld, D. A., Melnick, G. J., Sonnentrucker, P., et al. 2006, ApJ, 649, 816
Nisini, B., Lorenzetti, D., Cohen, M., et al. 1996, A&A, 315, L321
Nisini, B., Benedettini, M., Codella, C., et al. 2010, A&A, 518, L120
Nisini, B., Santangelo, G., Antoniucci, S., et al. 2013, A&A, 549, A16
Ray, T., Dougados, C., Bacciotti, F., et al. 2007, Protostars and Planets V, 231
Roelfsema, P. R., Helmich, F. P., Teyssier, D., et al. 2012, A&A, 537, A17
Santangelo, G., Nisini, B., Giannini, T., et al. 2012, A&A, 538, A45
Santangelo, G., Nisini, B., Antoniucci, S., et al. 2013, A&A, 557, A22
Suutarinen, A. N., Kristensen, L. E., et al. 2014, MNRAS, 440, 1844
Tafalla, M., Liseau, R., Nisini, B., et al. 2013, A&A, 551, A116
van der Tak, F. F. S., Black, J. H., Schöier, F. L., et al. 2007, A&A, 468, 627
van Dishoeck, E. F., Kristensen, L. E., Benz, A. O., et al. 2011, PASP, 123, 138
Vasta, M., Codella, C., Lorenzani, A., et al. 2012, A&A, 537, A98
Whittet, D. C. B., Prusti, T., Franco, G. A. P., et al. 1997, A&A, 327, 1194
Ybarra, J. E., & Lada, E. A. 2009, ApJ, 695, L120